

Exploring sulfate and metals removal from Andean acid mine drainage using CaCO_3 -rich residues from agri-food industries and witherite (BaCO_3)

Alfonso Larraguibel^{a,b}, Alvaro Navarrete-Calvo^{a,b}, Sebastián García^{b,c}, Víctor F. Armijos^d, Manuel A. Caraballo^{b,c}

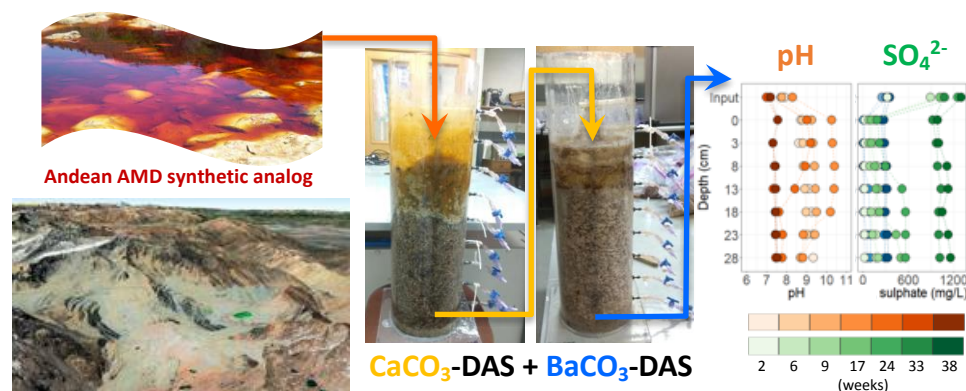
^aGeology Department, University of Chile, Plaza Ercilla 803, Santiago, Chile

^bAdvanced Mining Technology Center, University of Chile, Avda. Tupper 2007, 8370451 Santiago, Chile

^cMining Engineering Department, University of Chile, Avda. Tupper 2069, Santiago, Chile.

^dInnovation and Knowledge Department, Sacyr Chile, Isidora Goyenechea 2800, Santiago, Chile.

Graphical Abstract



Declaration of interest: None

Corresponding authors:

Manuel A. Caraballo and Alfonso Larraguibel

Phone: (+56) 2 29784479

E-mails: mcaraballo@ing.uchile.cl (Manuel A. Caraballo).

alfonso.larraguibel@ing.uchile.cl (Alfonso Larraguibel)

1
2
3
4
5
6
7
8
9
10
11
12
13
14
15
16
17
18
19
20
21
22
23
24
25
26
27
28
29
30
31
32
33
34
35
36
37
38
39
40
41
42
43
44
45
46
47
48
49
50
51
52
53
54
55
56
57
58
59
60
61
62
63
64
65

25 Highlights:

- 26 - Sea- and eggshells proven as suitable alternatives to limestone on DAS systems
- 27 - Water high alkalinity and low Al/Cu ratios generates malachite in CaCO₃-DAS columns
- 28 -Long-term removal of different loads of sulfate was achieved using BaCO₃-DAS columns
- 29 - BaCO₃-DAS upscaling is feasible under a circular economy strategy

31 Abstract:

32 Dispersed alkaline substrate (DAS) is a matured passive remediation technology that has shown
33 very high performances treating acid mine drainages (AMD). However, this remediation approach
34 needs to improve its environmental footprint as well as to ensure almost complete water sulfate
35 removals for long periods of time. The present study improves the use of witherite (BaCO₃) as a
36 reagent on DAS-type treatments to induce highwater sulphate removals in the context of Andean
37 AMD. Also, three CaCO₃-rich residues from the agri-food industry were tested as alternatives to
38 the current use of limestone. Two sets of column experiments were developed with various flow
39 rates (1.5-5.4 L/day), net acidities (202 and 404 mg/L as CaCO₃ eq.) and reactive agents (calcite,
40 eggshells, seashells and witherite). Seashells were validated as a perfect limestone substitutes on
41 the CaCO₃-DAS stages. Malachite was observed, for the first time within these columns, as a
42 mineral phase actively involved in Cu water removal. The BaCO₃-DAS columns achieved values
43 under 500 mg/L of sulfate at the output of the system for up to 6 months (initial sulfate
44 concentration ranged 1,234-2,468 mg/L). Upscaling calculations of the present results support the
45 feasibility of using this technology at a full field scale, especially as a wastewater treatment for
46 abandoned mine sites, although some strategies to reduce witherite costs are recommended.

48 **Keywords:** dispersed alkaline substrate, malachite, acid mine drainage, seashells, passive
49 treatment system.

1
2
3
4
5
6
7
8
9
10
11
12
13
14
15
16
17
18
19
20
21
22
23
24
25
26
27
28
29
30
31
32
33
34
35
36
37
38
39
40
41
42
43
44
45
46
47
48
49
50
51
52
53
54
55
56
57
58
59
60
61
62
63
64
65

58 1. INTRODUCTION

59
60 Acid mine drainage (AMD) is a specific type of water pollution resulting from its interaction
61 with sulfide minerals (mainly pyrite) at oxidizing environments (Dold, 2014). As a result, this
62 environmental problem is ubiquitously present around the world in mined and un-mined sulfide
63 rich rocks (Jacobs et al., 2014). These drainages are characterized by high metals and sulfate
64 concentrations and low pHs, making them extremely harmful for the environment, causing severe
65 biotic impairment (only extremophile forms of life like bacteria, fungus or algae remain present)
66 and making the waters unsuitable for other human uses (i.e., consumption, agriculture, farming,
67 ...)(Skousen et al., 2017; Younger and Wolkersdorfer, 2004; Akcil and Koldas, 2006).

68
69 Because of the severity and widespread distribution of this water pollution around the world, a
70 substantial amount of different remediation approaches has been generated during the last three
71 decades (Younger et al., 2002; Ziemkiewicz et al., 2003; Ayora et al., 2013). The most frequently
72 used treatments to remediate high flowrates of AMD are characterized by an intensive use of
73 energy to power the multiple mobile mechanical parts and electronical components of the
74 industrial treatment plants (Johnson and Hallberg, 2005; Kefeni et al., 2017), and for this very
75 reason this approach is typically referred as active treatments. The particular design of an active
76 treatment depends on both the specific water pollution to be treated and the water quality to be
77 achieved at the output of the system. Therefore, a variety of treatments units (e.g., neutralizing
78 reactors, softening reactors, filtration and/or reverse osmosis) are frequently connected in series to
79 achieve the desired water quality (Johnson and Hallberg, 2005, INAP, 2003). However, a common
80 denominator of most active treatments is the use of a neutralizing step to raise water pH and induce
81 the precipitation of metals, with lime ($\text{Ca}(\text{OH})_2$) as the most frequent chemical reagent. Active
82 treatments commonly require high maintenance, high chemical reagents and energy consumptions
83 and highly specialized operators, resulting in significant capital and operational (CAPEX and
84 OPEX) expenditures. Nowadays, they are used primarily in active mine sites (Johnson and
85 Hallberg, 2005).

86
87 On the other hand, there are the so-called passive treatments that use a different approach to
88 treat AMD with a minimal or none use of electrical energy. Those treatment technologies are
89 designed to favor the gravitational flow of the AMD through one or more different substrates
90 and/or steps designed to remove metals and/or sulfate and to increase water pH at the same time.
91 They commonly require important expenditures in the initial construction phase (land removal and
92 civil-engineering-type construction) but with a low maintenance, no energy consumptions and
93 without needing highly specialized operators during the operation of the plant, (high CAPEX but
94 low OPEX). The results are cheaper and more environmentally friendly options if compared with
95 active treatments (Skousen et al., 2017; Johnson and Hallberg, 2005; Gazea et al., 1996). However,
96 as a downside, they use to have some limitations regarding the metals and sulfate concentrations
97 of the inflowing AMD and substantial limitations considering AMD inflow rates (i.e., inflow rates
98 are typically lower than 50 L/s, depending on the water chemistry) (Ziemkiewicz et al., 2003;
99 Ayora et al., 2013; Skousen and Ziemkiewicz, 2005). Passive treatments can also be sub-divided

1
2
3
4 100 in two big categories: biogeochemical- (e.g., vertical flow reactors or aerobic and anaerobic
5 101 wetlands) or geochemical-based systems (e.g., anoxic limestone drainage or limestone permeable
6 102 barriers), and different hybrid options combining both of them (Skousen et al., 2017; Sheoran A.
7 103 and Sheoran V., 2006). Passive treatments systems may face several specific problems depending
8 104 on their individual design and geochemical or biogeochemical approach. Notwithstanding, most
9 105 of these treatments frequently suffer from two common problems: clogging (progressively
10 106 reducing the flowrate that the system can receive) and reactive material passivation (the reactive
11 107 material get isolated from the AMD by a cover of precipitates and loses its neutralizing
12 108 capacity) (Ayora et al., 2013; Simón et al., 2005; Rose et al., 2004).
13
14
15
16

17 110 On an effort to overcome the frequent clogging and passivation issues observed on most
18 111 traditional AMD passive treatment systems, the concept of Dispersed Alkaline Substrate (DAS)
19 112 was first introduced in 2006 (Rötting et al., 2006a; Rötting et al., 2006b). DAS consists on a
20 113 mixture of a coarse-grained inert material (to prevent clogging problems by the generation of a
21 114 high porosity substrate) and a fine-grained reactive material (to minimize passivation by enhancing
22 115 the reactive material dissolution rate) (Rötting et al., 2008a). This treatment technology has been
23 116 optimized and improved for more than a decade using mostly AMDs from the Iberian Pyrite Belt
24 117 (IPB, SW Spain) (Ayora et al., 2013; Caraballo et al., 2009; Caraballo et al., 2011; Macias et al.,
25 118 2012; Torres et al., 2018) but also from other countries around the world like Ecuador (Delgado et
26 119 al., 2019) and Canada (Rakotonimaro et al., 2016 and 2018). Those polluted waters are
27 120 characterized by very high to extreme metal and sulfate concentrations and low to very low pH
28 121 values (Table 1, input waters). Historical operational conditions and performances of the main
29 122 DAS-type treatment systems (i.e., laboratory column experiments, pilot plants and field full scale
30 123 treatment systems) has been summarized in Table 1 in order to identify the strengths and weakness
31 124 of this mature technology. Most laboratory and field experiments until 2018 were based on
32 125 different combinations of operational units using limestone sand (CaCO_3) and/or periclase dust
33 126 (MgO) as reagents to increase water pH. Typically, limestone dissolution increases water pH
34 127 around 6 and induces the removal of trivalent metals by the precipitation of schwertmannite
35 128 ($\text{Fe}_8\text{O}_8(\text{OH})_6\text{SO}_4 \cdot 5\text{H}_2\text{O}$) and hydrobasaluminite ($\text{Al}_4(\text{SO}_4)(\text{OH})_{10} \cdot 36\text{H}_2\text{O}$); whereas periclase
36 129 dissolution generates water pHs higher than 8.5 inducing the precipitation of divalent metals like
37 130 zinc (Zn^{2+}), manganese (Mn^{2+}), nickel (Ni^{2+}), cadmium (Cd^{2+}) or cobalt (Co^{2+}) (Table 1). Because
38 131 the well-known geochemical and mineralogical processes governing trivalent and divalent metals
39 132 removal (as well as some others metals and metalloids adsorption and/or co-precipitation) have
40 133 been extensively discussed in previous works (i.e., the substantial bibliography on Table 1), it was
41 134 decided not to repeat them in the present study and the reader is referred to the previous
42 135 bibliography for detailed information.”
43
44
45
46
47
48
49
50
51
52

53 137 Input and output net acidity (as mg/L of CaCO_3) can be used to evaluate the system remediation
54 138 performance since this parameter is calculated taking into consideration the five most relevant
55 139 elements controlling the AMDs hydrochemistry (i.e., aluminum Al, copper Cu, iron Fe, Zn and
56 140 Mn) as well as water pH and alkalinity values. All limestone- and/or periclase-based DAS
57 141 treatment systems achieved very good acidity removals, being able to reduce water net acidities
58 142 from values in the range of 1,500-5,000 mg/L as $\text{CaCO}_3\text{eq.}$ to net acidities at the systems outputs
59
60
61
62
63
64
65

1
2
3
4
5
6
7
8
9
10
11
12
13
14
15
16
17
18
19
20
21
22
23
24
25
26
27
28
29
30
31
32
33
34
35
36
37
38
39
40
41
42
43
44
45
46
47
48
49
50
51
52
53
54
55
56
57
58
59
60
61
62
63
64
65

143 on the range of 0 to 900 mg/L as CaCO₃eq. (depending on the specific experiment performance,
144 Table 1). It is important to highlight that the most recent experiences were able to optimize the
145 system performance and obtain net acidity values at the output of the systems close to 0 mg/L as
146 CaCO₃ eq. (i.e., experiences from 2012 to 2018, Table 1). However, all those treatments were
147 unable to significantly reduce sulfate water concentrations, achieving sulfate removals on the range
148 of 0% to 40% comparing input and output concentrations (Table 1).

14
15
16
17
18
19
20 149
21

Table 1: Historical operational conditions and performance of DAS-type treatment systems

Location		Monte Romero	Monte Romero	Monte Romero	Shillbottle	Mina Esperanza	Monte Romero	Monte Romero	Almagrera	Poderosa Mine	Mina Concepcion
Experiment Scale		Lab columns	Pilot plant	Pilot plant	Lab columns	Field full scale	Field Pilot plant	Lab columns	Lab columns	Lab columns	Field full scale
Input mean values	pH	2.80	3.30	3.08	3.90	2.65	3.58	2.70	2.60	2.40	2.70
	Al	106	75	117	200	147	80	128	251	532	119
	Fe	250	315	358	5	900	260	161	744	1052	286
	Zn	365	310	388	102	26	350	431	976	0.06	20
	Mn	22	20	19	77	5	13.50	18	467	0	N/A
	Cu	3.30	1.50	10	N/A	18	2.70	7	165	0.10	N/A
	SO ₄ ²⁻	3510	3200	3640	N/A	3900	3430	3500	11700	7532	N/A
Net Acidity	(mg/L of CaCO ₃)	1727	1500	2450	1500	2500	1609	1800	5000	5000	1300
Output mean values	pH	6.50	6	5.90	9.50	5.70	9.80	6.80	7.50	7.60	7.20
	Al	2	5.25	3.40	50	2	<0.2	0.26	0	0.10	dl
	Fe	2	237	83	0	600	<0.2	0	0	0.08	25
	Zn	350	294	279	20	15	<0.05	7.84	1.70	0	dl
	Mn	22	20	17	45	3	<0.2	3.38	14.50	0	N/A
	Cu	0.50	0.02	0.20	N/A	0.50	<0.01	0.03	0.05	0	N/A
	SO ₄ ²⁻	3500	3200	3500	N/A	3500	2800	3600	14400	22	N/A
Net Acidity	(mg/L of CaCO ₃)	500	630	632	400	900	0	20	30	0	50
Flow rate	(L/day)	0.14-1			1.50			1	1	0.40	
	(L/min)		1	1			1				
Residence Time	(L/s)					0.50					0.80
	(hours)	31-168	24	24 (Lim), 10 (Per)	12	54	36 (Lim), 12 (Per)	17	17	30	70-160
Duration	(months)	16	11	9	3	20	6	4.5	4.5	1.5	12
Reactive materials		Lim.	Lim.	Lim. & Per.	Per.	Lim.	Lim. & Per.	Lim. & Per.	Lim. & Per.	Lim. & With.	Lim. & Per.
References		Rotting et al., 2008a	Rotting et al., 2008b	Caraballo et al., 2009	Caraballo et al., 2010	Caraballo et al., 2011	Macias et al., 2012	Ayora et al., 2016	Ayora et al., 2016	Torres et al., 2018	Martinez et al., 2018

All locations are in the Iberian Pyrite Belt, SW Spain except for Shillbottle that is in NE England

Lim. = Limestone (CaCO₃); Per. = Periclase (MgO); With. = Witherite (BaCO₃)

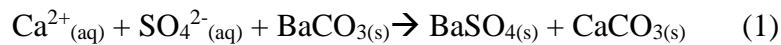
N/A: Not Analyzed or Not Available, dl: Detection Limit

Net acidity calculated as follows when not directly available: $50.045(3C_{Al}+2C_{Fe}+2C_{Mn}+2C_{Zn}+2C_{Cu}+10^{-pH})-alk.$ C_X: molar concentrations. Modified from Rotting 2008a to consider Cu.

61 150
62
63
64
65

1
2
3
4 151 Sulfate upper limit concentrations in water quality guidelines for irrigation or for drinking depend
5 152 on each country environmental legislation but typical values are on the ranges of 150-1000 mg/L
6 153 and 250-500 mg/L, respectively (Valenzuela, 2019); whereas AMD waters, at the IPB, treated by
7 154 limestone- or periclase-based DAS treatments systematically show water sulfate concentrations
8 155 higher than 3,000 mg/L (Table 1).
9
10
11 156

12 157 To tackle the sulfate problem, witherite (BaCO_3) was recently tested at laboratory scale as a
13 158 possible new alkaline reagent substituting limestone or periclase (Torres et al., 2018). Witherite
14 159 dissolution induces sulfate precipitation as barite (BaSO_4) according to the following reaction:



20 162
21 163 Witherite dissolution also increase AMD pH to values around 7 or 8 with the concomitant
22 164 precipitation of any remnant trivalent metals in solution as well as some divalent metals too (Torres
23 165 et al., 2018). This recent experiment showed promising results, inducing almost complete sulfate
24 166 removal and complete net acidity removal (Table 1). However, this exploratory experiment only
25 167 last one month and a half, used a very low inflow rate (0.4 L/day) and was tested at extreme net
26 168 acidity conditions (5,000 mg/L as CaCO_3). Consequently, the obtained results should not be
27 169 applied directly to other realities characterized by higher flowrates and lower acidities (like the
28 170 one tested on the present study). Even more importantly, the shortness of the experiment
29 171 discourages to extrapolate results to operation times longer than a couple of months.
30
31
32 172

33 172
34 173 In addition, a recent life cycle assessment study performed on the field full scale DAS passive
35 174 treatment at Mina Concepción, SW Spain (Martínez et al., 2019), revealed that the use of limestone
36 175 from a quarry had a substantial impact on its carbon and ecological footprint. This is due not only
37 176 to the typical long distances from limestone quarries to mineralized regions where AMD
38 177 treatments use to be needed, but also from the mining operation at the quarry. On this respect, the
39 178 reuse of alternative by-product or residues (instead of mining raw materials) should be encouraged.
40 179 For instance, seashells are being used to substitute other alkaline materials in very different
41 180 applications like aggregate in plain concrete (Martinez-Garcia, 2017 and 2019) or adsorbent in
42 181 AMD treatments (Bavandpour, 2018). Bivalve mollusks represent almost 10% of the world's total
43 182 fishery production, being 26% of the entire volume (Martinez-Garcia, 2019). China is by far the
44 183 leading producer of bivalve mollusks (10.35 million tons in 2015), followed by far by Japan
45 184 (819,131 tons in 2010), the United States (676,755 tons), the Republic of Korea (418,608 tons),
46 185 Thailand (285,625 tons), France (216,811 tons) and Spain (206,003 tons). Other main bivalve-
47 186 producing countries are Canada, Chile, Italy and New Zealand (FAO 2018). Regarding eggshell
48 187 availability, China (the biggest world consumer) and Chile (a small world consumer) consumed
49 188 roughly 26.4 million tons and 175,000 tons of eggs in 2013 (FAOSTAT). In other words, they
50 189 generated 2.9 million tons and 19,000 tons of eggshells (considering that eggshells typically
51 190 represent a 11% of the egg's total weight). Therein, these residues from the agri-food industry
52 191 could be considered as worldwide distributed and available alkaline replacement.
53
54
55
56
57
58
59 192
60 193
61
62
63
64
65

1
2
3
4 194 Also, it is important to consider that all experiments, but the one in 2010 using the AMD from
5 195 Shillbottle (UK), were performed using AMDs with very high to extreme metal and sulfate
6 196 contents and the applicability and performance of this technology at lower metal and sulfate
7 197 concentrations have not been properly studied (Table 1). These AMDs with lower metal and sulfate
8 198 concentrations are very typical in many mining regions (e.g., porphyry copper deposits, coal
9 199 deposits, etc.) around the world that could benefit from the implementation of an optimized DAS
10 200 technology.
11
12
13
14 201

15 202 The main scopes of the present study are: 1) to investigate different options of potentially more
16 203 sustainable alkaline materials to replace limestone from quarries, 2) to optimize the best sequence
17 204 of DAS passive treatment steps to treat AMDs with low to medium acidity (< 500 mg/L as CaCO₃
18 205 eq.) and sulfate (< 2,000 mg/L) contents if compared with previous experiences (Table 1), and 3)
19 206 to evaluate the use of witherite to remove variable sulfate loads during periods of treatments
20 207 significantly longer (i.e., higher than half a year) than the forty days used in the only previous
21 208 study.
22
23
24 209

26 210 **2. MATERIALS AND METHODS**

28 211 *2.1 Chilean and Argentinian AMDs as possible low acidity AMD proxies*

30 212
31 213 As mentioned on the introduction section, DAS passive treatment technology has been
32 214 successfully used to remove di- and tri-valent cations from highly polluted AMDs, but its
33 215 performance on less concentrated AMDs is still pending. Although an efficient and positive
34 216 applicability of this technology to less polluted waters can be anticipated, its specific
35 217 implementation is not straightforward because a few operational parameters must be optimized
36 218 and its working ranges defined (i.e., residence time, flowrate that can be treated, metal removal
37 219 efficiency and duration of the reactive material prior to its passivation or its total consumption).
38 220 On this respect, it was decided to perform an exploratory bibliographic study of reported AMD
39 221 waters in the Andes (mostly in Chile and Argentina) to obtain a broad picture of the type of low to
40 222 medium AMD polluted waters developed on this geological setting. In this part of the Andes, the
41 223 mine industry is heavily focused on Cu extraction and the most common mineral deposits (and
42 224 residues) include porphyry copper, iron oxide-copper-gold ore deposits (IOCG) and/or iron oxide-
43 225 apatite ore deposits (IOA), and Stratabound (Camus and Dilles, 2001; Barra et al., 2017).
44
45
46
47
48
49 226

50 227 In an attempt to characterize AMD flows in Chilean and Argentinean Andes, 296 samples
51 228 analyses from 32 different field sites were gathered on a database (Table S1, Supplementary
52 229 Information). The statistical distribution of the samples and the main statistics are shown in table
53 230 S1. The original synthetic AMD (AMD 1x, Figure 1) used in the lab experiments was created to
54 231 reproduce the water chemistry of a real sample with a net acidity value close to percentile 75 of
55 232 the generated database (line 171 highlighted on green on Table S1, Supplementary Information).
56 233 By doubling the concentrations of the original synthetic AMD, (AMD 2x, Figure 1) a net acidity
57 234 of 404 mg/L as CaCO₃eq. was obtained. This new synthetic AMD has a net acidity value close to
58
59
60
61
62
63
64
65

percentile 90 of the created database of Andean AMDs from Chile and Argentina. Therefore, the present lab experiments will potentially have direct application to most AMDs in our database.

2.2 Experimental design

To achieve the main goals of the present study, a sequence of two different sets of laboratory experiments were designed and implemented (CaCO₃-DAS and CaCO₃-DAS+BaCO₃-DAS Experiments in Figure 1).

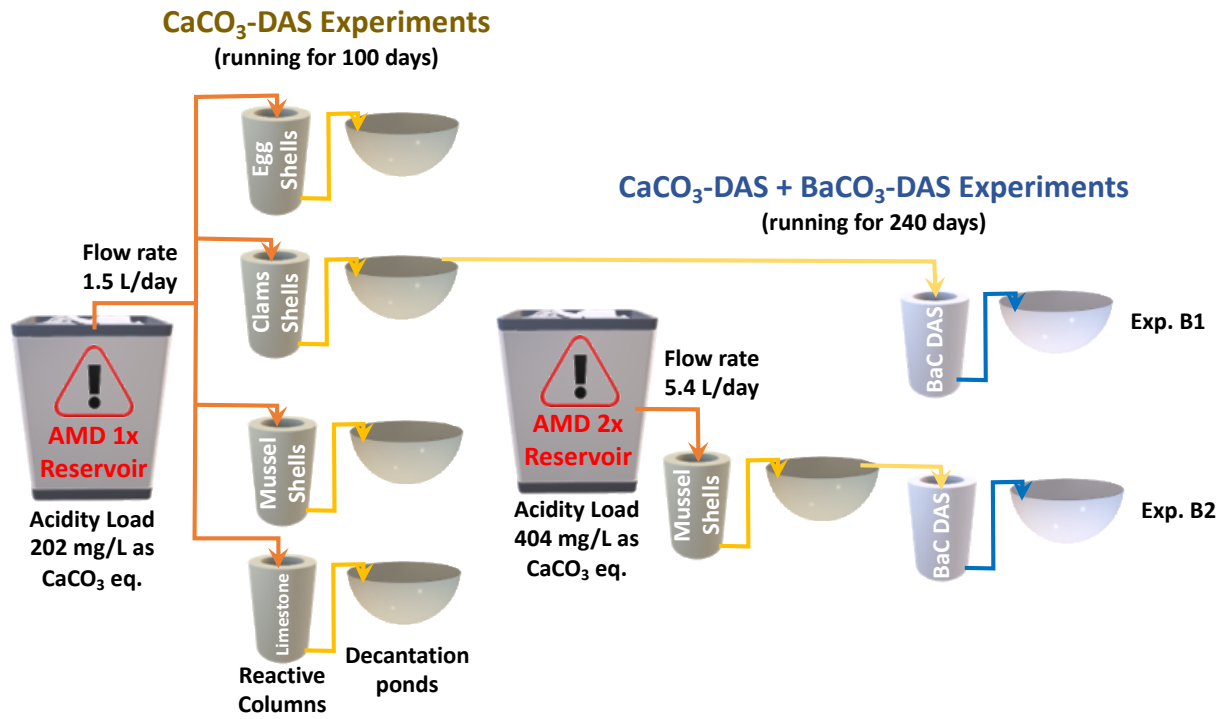


Figure 1: Experimental design showing the three different experimental setups implemented. The composition of the AMD (mark as x on the graphic) is shown in detail on Table A.1 (Appendix). This composition is multiplied by 2 to generate the second AMD reservoir.

During the first experiment, four different calcium carbonate (CaCO₃) reagents were tested to evaluate the possible substitution of commercial limestone (traditionally used in all previous field and laboratory DAS studies and obtained from the closest available quarries) by a potentially more sustainable material (i.e., an industrial residue that could be reused and re-conceived as a by-product rather than as a residue). Limestone was bought at a local supplier while eggshells and seashells were acquired (as waste products, no cost) in local poultry and seafood local markets. All materials were hand crushed using an agate mill and sieved under 4mm. At the same time, the DAS system performance treating an Andean AMD with moderate metals and sulfate concentrations were tested. All the columns were fed for 100 days using the synthetic AMD previously mentioned (Table A.1) and a flow rate of 1.5 L/day. This flowrate was selected to obtain a water residence time within the columns around 48 hours to favor an optimal operation of the

DAS technology, and it was done following the recommendations of a previous study that discussed in detail the optimal working conditions for this type of technology (Ayora et al., 2013). All columns had 50% porosity and a water residence time of 48h. Reactive material to wood shavings volumetric ratio was 1 to 4 within the calcite-DAS and clams shells-DAS columns and 1 to 5 within the mussel shells-DAS and eggs shells-DAS columns. Notice that all the columns on this and the following experiments are followed by a decantation/reaction pond, which are designed to ensure the needed time for the water to equilibrate and complete the mineral precipitation reactions involved in the water treatment. Additional details about the columns and decantation ponds setups and construction can be found in the supplementary information (Fig. A.1 and A.2, Appendix).

The second experiment was focused on the assessment of different operational parameters affecting sulfate removal using BaCO₃-DAS columns on long term experiments. On this respect, AMDs with two different concentrations (x and 2x, Fig. 1 and Table A.1) were fed to two different columns using two different inflow rates (1.5 and 5.4 L/day, Table 2). These flowrates were selected to test the effect of high versus low residence times within the columns (48 vs 13.5 hours), as well as to study BaCO₃-DAS columns performance under two different sulfate loads (i.e., 1.9 and 13.3 g/day). This last experiment was maintained for 8 months to clearly evaluate the system performance during long periods of time.

Table 2: Main operational conditions of the different columns setups in the experiments including a BaCO₃-DAS step

	Net acidity (mg/L of CaCO ₃) [*]	SO ₄ ²⁻ (mg/L)	Flow rate (L/day)	SO ₄ ²⁻ load (g/day)	Acid load [#]	Columns residence time (h)	Total duration (months)	Columns reactive materials	Reactive/inert material proportions
Experiment B.1	202	1234	1.50	1.90	53.86	48	8 [§]	Clams shells →Witherite	16/84 (v/v) 1/1 (w/w)
Experiment B.2	404	2468	5.40	13.30	387.84	13.50	8	Mussels shells →Witherite	20/80 (v/v) 2/1 (w/w)

* Net Acidity=50.045(3C_{Al}+2C_{Fe}+2C_{Mn}+2C_{Zn}+2C_{Cu}+10^{pH})-alk. C_X: molar concentrations. Modified from Rotting 2008a to consider Cu.

Calculated as (flow rate*net acidity)/(1000*horizontal treatment area).

§ It is important to keep in mind that the CaCO₃-DAS columns have an extra 100 days in these experiments.

2.3 Sampling and analysis

Water samples were collected (using lateral sampling ports as well as input and output waters) on a monthly base (or shorter) during the operation time of the different experiments. Filtered samples (filter pore size of 0.45 μm) were acidified with HNO₃ until reaching a pH value close to 1 and stored at the refrigerator at 4°C until analysis. The chemical analyses were performed by ICP-MS and ICP-OES at external analytical company (i.e., Bureau Veritas/Acmelabs) using a commercial analytical package (i.e., ICP-MS S0200 analysis for natural waters). Additional details about the analytical method can be found in the supplementary information (Appendix A). The detection limits achieved are lower than the regulatory limits proposed by the World Health

1
2
3
4 292 Organization (WHO, 2008) and the US Environmental Protection Agency (USEPA, 2017).
5 293 Specific values for these limits are shown in Figure A.3 (Appendix).
6
7 294

8 295 Physicochemical parameters such as pH, redox potential (Eh), dissolved oxygen (OD) and
9 296 electric conductivity (EC) were measured using a Thermo Orion Star A329 portable meter, with
10 297 the following electrodes: For pH Orion 8107UMMD, for ORP measurements Orion 9179BN, for
11 298 EC Orion 013010MD and for OD Orion 087003. The calibration solutions used were: Orion pH
12 299 buffers 910104 (pH 4.01), 910107 (pH 7), 910110 (pH 10.01), ORP standard Orion 967961, EC
13 300 standards Orion 011007 and Orion 011006. All electrodes were properly calibrated before each
14 301 measurement campaign.
15
16 302

17 303 Solid samples were taken at the end of each experiment, every 4cm in the upper segment of the
18 304 substrate and every 6cm afterwards. An additional sample for each column was taken on the
19 305 surface (5mm). The samples were oven-dried (Oven Memmert UN-110) at 30°C for 3-4 days,
20 306 milled using an agate mortar and pestle and finally then sieved under 75µm.

21 307 The semi-quantitative mineralogical analyses of the solid samples were obtained using powder
22 308 X-ray diffraction (XRD) of randomly oriented samples on Bruker D5005 X-ray diffractometer
23 309 with CuK α radiation. Diffractometer settings were: 40 kV, 30 mA and a scan range of 10–63° 2 θ ,
24 310 0.02° 2 θ step size, and 5 s counting time per step. The obtained diffractograms were analyzed using
25 311 the software X PowderX[®] and PDF2 database (Figure 3 and Figures A.4 and A.5 on the Appendix).
26 312 Fluorite was added to the samples as internal standard to correct any possible drifting of the
27 313 diffractograms and to improve the calculations of the mineral's concentrations. More detail about
28 314 the specific analysis procedure are offered in the Appendix.
29
30 315

31 316 Electron microscopy images and chemical analyses by energy dispersive spectroscopy were
32 317 obtained with a SEM-EDS FEI Quanta 250. Samples were analyzed using three different detectors:
33 318 ETD (Everhart Thornley detector), BSED (Backscattered electron detector) and EDX (Energy
34 319 dispersive x-ray). The instrument was operated using a Voltage range of 10kv to 30kv. The images
35 320 were processed using the Quanta 250 interface whereas the EDX analysis were studied using the
36 321 software INCA[®].
37
38 322

39 323 *2.4 Hydrogeochemical Model*

40 324 The geochemical model was implemented using the open source geochemical software
41 325 (PHREEQC) which is a powerful reaction-based software with a long tradition in the fields of
42 326 mining and environmental engineering studies (Parkhurst and Appelo, 2013). Detailed
43 327 explanations of the conceptual geochemical models used as well as the specific chemical reactions,
44 328 kinetic equations, mineral equilibrium phases, and cells dynamic characteristics during the reactive
45 329 transport model are offered in the Supplementary Information (Tables A.2, A.3 and A.4).
46
47 330

48 331 **3. Results and Discussion**

49
50
51
52
53
54
55
56
57
58
59
60
61
62
63
64
65

332 *3.1 Assessment of CaCO₃ rich residues from agri-food industries treating an Andean AMD with*
 333 *intermediate metals and sulfate concentrations*

334 As previously mentioned, the first experiment was designed to evaluate: 1) the possible
 335 substitution of commercial limestone by a potentially more sustainable material and, 2) the DAS
 336 system performance when treating an Andean AMD with moderate metals and sulfate
 337 concentrations. Taking into consideration the singularities of the Chilean geography and its
 338 industrial matrix, it was decided to test two different types of seashells (clams and mussels shells)
 339 as well as eggshells. These materials are very common residues from the Chilean agri-food
 340 industries that can be easily found in big amounts on various locations along the country.

342 As can be observed in Table 3 all experiments showed a very similar performance, achieving
 343 almost complete removal of all trivalent metals (i.e., Fe and Al) as well as very high removals for
 344 Cu and Zn. The concentrations accomplished by these four elements are under the limits proposed
 345 by the World Health Organization (WHO, 2008) and the US Environmental Protection Agency
 346 (USEPA, 2017). On the other hand, no significant removal of Mn and sulfate was achieved and
 347 their concentrations in the outflowing waters are over the limits proposed by the WHO and the
 348 USEPA. Regarding final water pH only small differences were observed, ranging all the
 349 experiments between 6.8 and 7.3. So, if the performance of each different reagent is evaluated in
 350 terms of metal removal and pH increase, all of them are equally efficient and any of them could
 351 potentially be used as neutralizing agent during the CaCO₃-DAS step of the passive treatment.
 352 However, subtle slower dissolution kinetics and lower final pHs can be observed if limestone and
 353 eggshells results are compared with the ones obtained for seashells (clams and mussels, Fig. A.6,
 354 Appendix). For all these reasons, it was decided to select seashells as the optimum CaCO₃ reagent
 355 to be used in the following experiments.

357 Table 3: Mean output water quality parameters from the 4 experiments performed to test different CaCO₃ reagents.
 358 The values recommended by the World health Organization (WHO, 2008) and the US environmental Protection
 359 Agency (USEPA, 2017) are also listed as references.

Reagent	pH	Fe(mg/L)	Al (mg/L)	Cu (mg/L)	Mn (mg/L)	Zn (mg/L)	SO ₄ ²⁻ (mg/L)	Net acidity (mg/L of CaCO ₃)*
Limestone	6.81 ± 0.08	0.125 ± 0.11	0.03 ± 0.01	0.015 ± 0.01	7.24 ± 0.43	0.99 ± 0.50	1179 ± 148	14.91 ± 1.36
Mussels Shells	7.34 ± 0.07	0.1 ± 0.14	0.03 ± 0.01	0.01 ± 0.01	6.63 ± 1.13	0.91 ± 0.66	1281 ± 336	13.89 ± 2.69
Clams Shells	7.34 ± 0.02	0.13 ± 0.16	0.03 ± 0.01	0.01 ± 0.01	5.86 ± 1.42	0.81 ± 0.33	1242 ± 293	12.38 ± 2.75
Egg Shells	7.11 ± 0.07	0.11 ± 0.11	0.02 ± 0.01	0.01 ± 0.01	6.99 ± 0.56	0.14 ± 0.04	1328 ± 231	13.33 ± 1.18
WHO-USEPA		0.30	0.10	2	0.05	5	250	

* Net Acidity=50.045(3C_{Al}+2C_{Fe}+2C_{Mn}+2C_{Zn}+2C_{Cu}+10^{-pH})-alk. C_X: molar concentrations. Modified from Rotting 2008a to consider Cu.

The values after the ± symbols correspond to the standard deviation of the mean values.

362 The detailed geochemistry controlling Fe and Al precipitation down the column's profiles
 363 (Fig.A.6, Appendix) showed the same trends confirmed in many previous studies (i.e., an upper

iron precipitation front controlled by schwertmannite followed by an aluminum precipitation front controlled by hydrobasaluminite, Caraballo et al., 2009). Therefore, it will not be discussed again on this work. However, the new AMD compositions used on the present experiments, more specifically the different ratios between dissolved elements and particularly the low Al/Cu ratio (Table S6, Supplementary Information), induced a geochemical trend for Cu never observed before. This new Cu behavior was almost identical regardless the reactive material employed in the CaCO₃-DAS columns. Because of that and to avoid unnecessary redundant information, the following discussion will be focused just on the evolution of the geochemical profile of one selected column. To this end, the first column on experiment B.2 (Figure 1) was selected because the higher Al and Cu load used in this experiment could allow the better development of two differentiated precipitation fronts for these two elements.

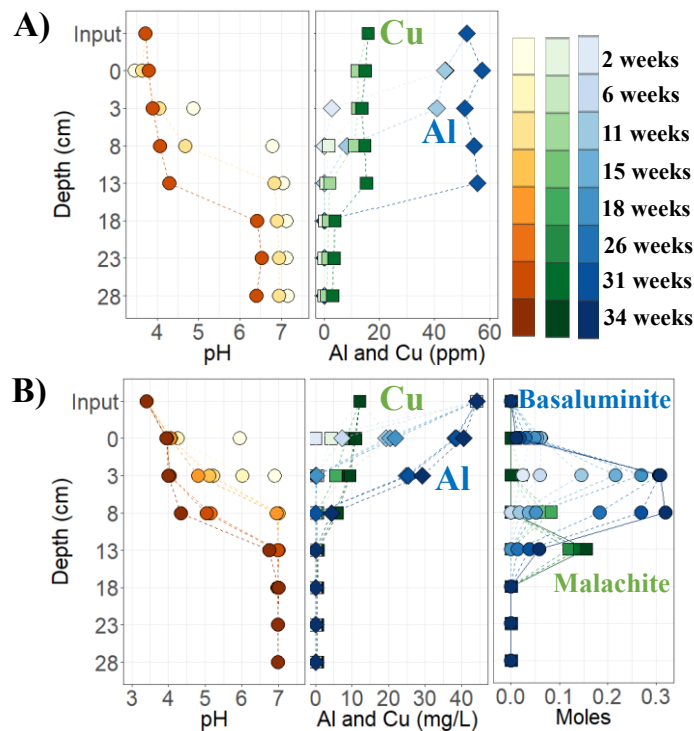


Figure 2. All the results correspond to the mussel shell-DAS column at experiment B.2. A) Spatial and temporal evolution of some representative operational parameters along the column, and B) Results obtained in the geochemical model performed with Phreeqc.

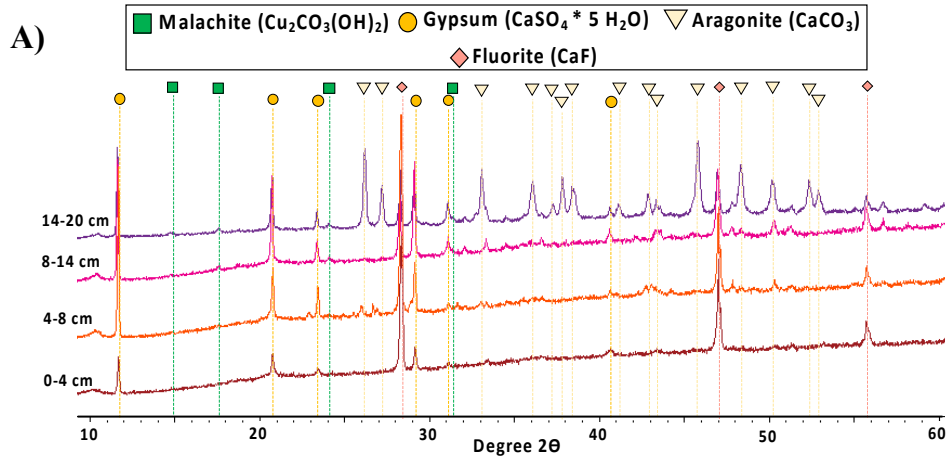
Previous studies have shown that copper precipitation typically mimics the precipitation profile showed by aluminum within the limestone-DAS columns (Ayora et al., 2013; Caraballo et al., 2009). This coupled behavior has been interpreted as Cu co-precipitation and/or sorption in hydrobasaluminite (Caraballo et al., 2009). However, the profiles obtained in the present experiments cannot be exclusively explained by these processes, because sometimes, Cu total removal is obtained deeper in the column profile and after complete Al removal is achieved (Figure 2.A). Additionally, the results of a geochemical model perform to this mussel shells-DAS column

1
2
3
4
5
6
7
8
9
10
11
12
13
14
15
16
17
18
19
20
21
22
23
24
25
26
27
28
29
30
31
32
33
34
35
36
37
38
39
40
41
42
43
44
45
46
47
48
49
50
51
52
53
54
55
56
57
58
59
60
61
62
63
64
65

389 anticipate the formation of a Cu precipitation front (made by malachite, $\text{Cu}_2\text{CO}_3(\text{OH})_2$) right
390 downward the hydrobasaluminite precipitation front (Figure 2B).

391
392 To confirm or deny the precipitation of malachite within the CaCO_3 -DAS columns (as well as the
393 presence of other mineral phases), several mineralogical analyses were performed (Figure 3).
394 Before that, a visual inspection of the DAS material during the solid sampling campaign revealed
395 the expected “colored precipitation zone”, showing the typical upper orange-reddish zone
396 approximately from 0 to 5 cm depth (and made by precipitated schwertmannite) followed by a
397 whitish zone roughly from 5 to 15 cm depth (made by hydrobasaluminite precipitates). A picture
398 of the column just before the solid sampling campaign is shown in Figure A.7 (Appendix). If some
399 solid samples from the deeper section of the column are looked closely, small particles (shell and
400 wood shaving pieces) coated with a green mineral can be observed (Fig. A.8, Appendix). These
401 green crystals were separated from the main grain, and fizziness was observed when they were put
402 in contact with a drop of 10% HCl (the expected reaction for malachite).

403
404 As in most previous studies, the XRD study of the remaining CaCO_3 -DAS is characterized by an
405 upper section (approximately down to 15-20 cm depth in this experiment) where the alkaline
406 reagent (i.e., aragonite, CaCO_3) has been consumed and the only clearly discernible XRD signals
407 (Fig. 3A) correspond to gypsum ($\text{CaSO}_4 \cdot 5\text{H}_2\text{O}$). Also, as usual, the diffractogram showed the
408 typical high background and/or noise due to the presence of a big amount of very poorly crystalline
409 phases like schwertmannite and hydrobasaluminite. However, three very subtle peaks
410 corresponding to malachite were identified on samples at 8-14 cm and 14-20 cm deep (Fig. 3A).
411 The semiquantitative study performed to this sample is in accordance with the previous visual
412 observations and the expected amount of malachite in both samples should be lower than 1% (Fig.
413 3B). Finally, the presence of malachite was also suggested by the data obtained using electron
414 microscopy, where single particles made by Cu, C and O (detected by EDS) were observed (Fig.
415 3C).



B)

Depth (cm)	Fluorite	Gypsum	Malachite	Aragonite	Amorphous
	(wt %)				
0-4	10.3	1.0			88.6
4-8	9.8	1.7			88.5
8-14	10.0	5.1	0.7		84.2
14-20	9.5	4.8	0.9	19.4	65.4

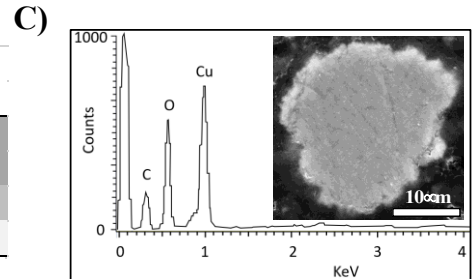


Figure 3. Mineralogical and chemical evidences of the presence of malachite within mussel shell-DAS column at experiment B.2. A) Stacked X-Ray diffractograms and mineral peaks assignment; B) Mineral semi-quantification using fluorite as internal standard; and C) EDS pattern and SEM electron backscattered image of a malachite single particle.

The most plausible reasons behind the precipitation, for the first time, of malachite in CaCO_3 -DAS type columns are: 1) the significantly low Al/Cu ratio in the AMD used in the present experiments (Table A.5) and 2) the higher alkalinity achieved in these experiments (around 300 mg/L as CaCO_3) comparing with other previous experiments (e.g., alkalinity in Monte Romero was around 100 mg/L as CaCO_3 , Caraballo et al., 2009) where no malachite was detected.

3.2 Evaluation of the long-term removal of different loads of sulfate using BaCO_3 -DAS

The only previous experience using witherite to remove SO_4^{2-} from AMD waters reported very promising results, showing an almost complete SO_4^{2-} water removal after the treatment (Torres et al., 2018). However, it is important to notice the low water inflow and operation time of the experiment (Table 1), as well as the intermediate sulfate concentration of the water entering the BaCO_3 -DAS column (i.e., from the 5,000 mg/L of sulfate in the original AMD only 1,770 mg/L exits the CaCO_3 -DAS column and enters the BaCO_3 -DAS column). As a result, the BaCO_3 -DAS column was submitted to a very modest sulfate load (0.7 g of SO_4^{2-} per day) on this experiment. To get a better understanding of the BaCO_3 -DAS technology response when submitted to higher sulfate loads, the BaCO_3 -DAS columns of the present study were designed to received 1.9 and 13.3 g/day of SO_4^{2-} (i.e., 2.7 and 19 times more sulfate than the experiment by Torres et al., 2018).

To facilitate the explanation of the main findings during these multiple experiments, the results from experiment B.1 (sulfate load of 1.9 g/day) will be used to exemplify the general geochemical performance of the BaCO₃-DAS columns. According to equation (1) the main expected effects of witherite dissolution should be an increase on water pH and a decrease on sulfate concentration. In addition, the waters may also exhibit a local increase in the concentration of barium (Ba, depending on the local final balance between witherite dissolution and barite precipitation) as well as some local decrease in Ca concentration as a result of CaCO₃ precipitation. Taking into account all these processes, it can be inferred that the BaCO₃-DAS column on experiment B.1 showed signs of witherite dissolution during the first 6 months of operation (Fig. 4A). During this period, the water outflowing the column always showed sulfate concentrations lower than 500 mg/L. However, if the geochemistry time series of the column are observed in detail, it can be observed how after 17 weeks of operation the sulfate concentration began to increase as water pH and exceeding dissolved Ba starts to decrease upward from the bottom of the column (Fig. 4A). This peculiar behavior cannot be explained by witherite exhaustion. As shown in the hydrochemical model performed (Fig. 4B), if the column would have progressively consumed the available witherite downward the column (as it did for the CaCO₃-DAS columns and during the early weeks of the BaCO₃-DAS experiments), it should have shown better sulfate removal and more steady water pHs (between 8 and 9) along the 38 weeks of the experiments.

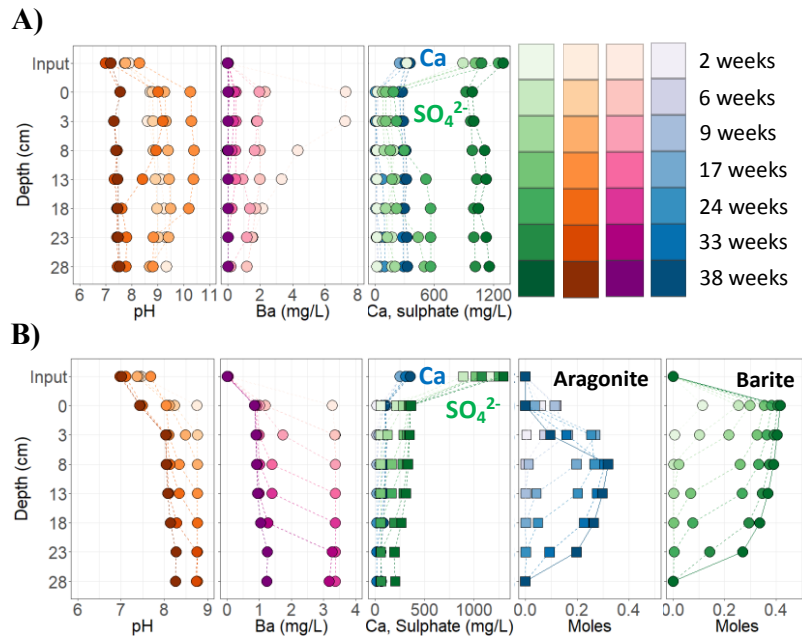


Figure 4. Raw (A) and modeled (B) hydrochemical depth profiles of the main operational parameters and elements within the BaCO₃-DAS column in experiment B.1. Notice that modeled precipitation profiles of barite (BaSO₄) and aragonite (CaCO₃) are shown in B), where positive values correspond to precipitated amount of mineral.

Also, it is important to notice that this evolution of the hydrochemical depth profiles is much faster in the BaCO₃-DAS column at experiment B.2 (Figure A.9.B, Appendix). Because of the higher sulfate load received by this column (13.3 g/day), the first signs of the reactive material exhaustion were observed after 11 weeks of operation and the remediation capacity of the column completely stopped after 18 weeks of operation. In addition, these figures show how both BaCO₃-

1
2
3
4
5
6
7
8
9
10
11
12
13
14
15
16
17
18
19
20
21
22
23
24
25
26
27
28
29
30
31
32
33
34
35
36
37
38
39
40
41
42
43
44
45
46
47
48
49
50
51
52
53
54
55
56
57
58
59
60
61
62
63
64
65

467 DAS columns achieved an excellent Mn removal when witherite dissolution is actively occurring.
468 Therefore, by using witherite the need of a MgO-DAS step to remove divalent metals (like Mn²⁺)
469 could be avoided.

470
471 To obtain a different perspective helping to explain the geochemical evolution of the column,
472 several solid samples at different depths within the column were obtained and studied by XRD.
473 During this solid sampling campaign, a visual inspection of the two BaCO₃-DAS columns allowed
474 identifying two well differentiated vertical zones. The first zone (wall zone) corresponded to the
475 reactive material close to the wall in contact with the inflowing water (notice that the design of the
476 column induced that the inflowing water run down the wall of the column instead of directly
477 dripping to the supernatant of the column, Figure A.10). The second zone (core zone) corresponded
478 to most of the column and it is characterized by a less cemented less compacted material (if
479 compared with the samples from the wall zone). The semiquantitative mineralogical
480 characterization of these samples are shown in Table 4. As it can be observed, all the columns and
481 sections are characterized by and almost complete or complete exhaustion of the original witherite
482 as well as by the significant precipitation of CaCO₃ mineral phases (i.e., calcite and/or aragonite)
483 and barite (Fig. A.4 and A.5, Appendix). Both BaCO₃-DAS columns typically show higher
484 amounts of CaCO₃ precipitates (calcite+aragonite) in the samples from the wall section (if
485 compared with the sample from the core section). These results are in accordance with the visual
486 observations during the sampling and could explain the higher cementation of the samples from
487 the wall section. It is also important to notice that the BaCO₃-DAS column at experiment B.2
488 showed no signs of witherite in the wall section whereas some remaining witherite was detected
489 in the samples from the core section.

Table 4. Mineralogical identification and semi-quantification of selected samples along the depth profile of the BaCO₃-DAS columns in experiments B.1 and B.2. Within each identified mineral, higher color intensity indicates higher mineral concentration, and viceversa.

Experiment	Depth (cm)	Fluorite	Barite	Calcite	Aragonite	ΣCaCO ₃ (wt %)	Witherite	Amorphous
B.1	0-4	10.0	5.5		1.4	1.4	2.4	80.7
	4-8	9.5	1.2		4.0	4.0	1.1	84.3
	13-18	10.2	1.1		4.1	4.1		84.5
B.1_Wall	0-4	10.6	2.3		10.8	10.8	2.3	74.0
	4-8	10.8	1.8		8.7	8.7	3.8	74.9
	13-18	10.3	1.2		2.8	2.8	1.9	83.9
B.2	0-4	9.7	0.8	1.0	1.8	2.8	2.4	88.6
	4-8	10.6	9.1		2.2	2.2	1.1	88.5
	13-18	10.7	13.0		3.1	3.1	1.0	84.2
	23-30	9.6	2.2	2.1		2.1	2.7	65.4
B.2_Wall	0-4	10.9	5.2	0.7	0.5	1.2		84.2
	4-8	10.2	6.3	0.7	1.0	1.8		76.9
	13-18	9.6	1.5	2.0	4.2	6.1		72.2
	23-30	9.6	2.9	3.9		3.9		83.3

ΣCaCO₃ = addition of calcite and aragonite concentrations (wt %). B.1 and B.2 correspond to samples obtained from the core of the column, whereas samples B.1_Wall and B.2_Wall were obtained close to the wall of the columns.

Another independent observation that could help explaining the geochemical behavior of the columns, is that during the columns operations they did not show any clogging problem (i.e., the inflow rate was kept constant and the water supernatant did not need to increase its hydraulic head to maintain the same outflow rate), despite the important mineral precipitation within the columns. In addition, a different coloring of the reactive material within the columns was developed during the experiment. At the end of the experiment, it was possible to clearly differentiate the wall and core sections within the column (the wall section went darker whereas the core section maintained the original coloring of the reactive mixture).

Considering all these independent observations, the following plausible interpretation for the column geochemical behavior and evolution is offered: During the first months of operation (i.e., 24 and 11 weeks at experiment B.1 and B.2, respectively) the BaCO₃-DAS columns showed signs of witherite dissolution and accomplished sulfate output concentrations lower than 500 mg/L. However, these columns began to exhibit the effect of preferential flows and water mixing a few weeks earlier. As a result, from the sixth (B.1) and fourth (B.2) months to the last of the experiments the columns lost their remediation capacities, but they maintained their original hydraulic conductivity due to the generation of preferential flow paths.

Moreover, the experimental design allowed gaining a better understanding of the BaCO₃-DAS technology regarding its sulfate removal efficiency and lifetime. The information is graphically presented on Figure 5, but it is also shown *in extenso* in the Supplementary Information (Table S7). Comparing the results in figure 5, it can be observed how an increase in the sulfate load

received by the columns implied a decrease in their lifetime (i.e., moment when the water outflowing the column reach a value higher than 500 mg/L, yellow circles on the figure). On the other hand, the BaCO₃-DAS column in experiment B.2 was able to achieve a higher accumulated removed sulfate load during its shorter operation time but it has to be considered that a double amount of witherite (i.e., 2kg instead of 1kg) was used on this experiment.

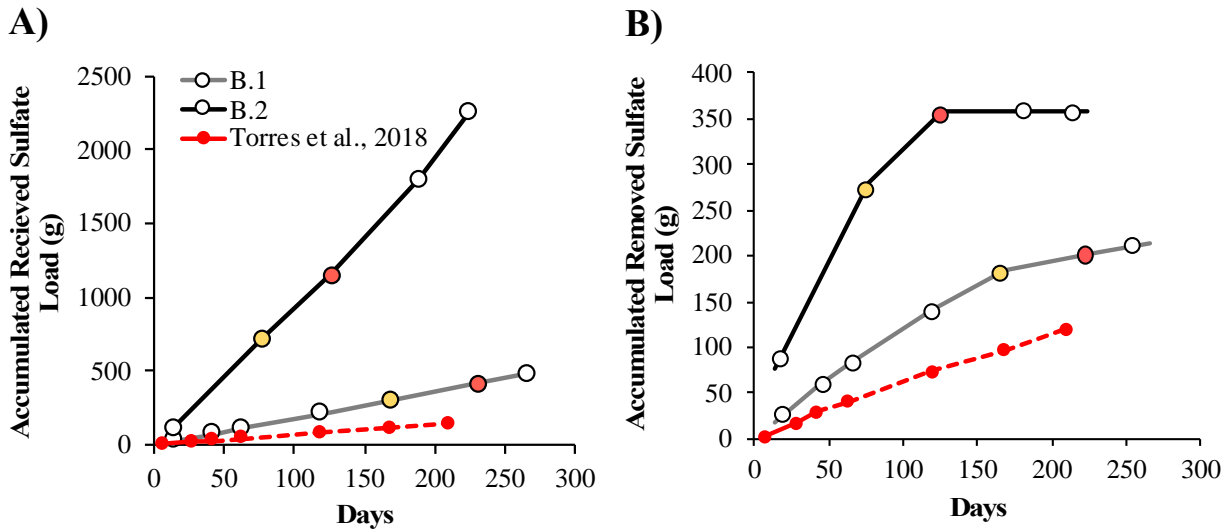


Figure 5. A) Accumulated received sulfate load and B) accumulated removed sulfate load in the two tested BaCO₃-DAS columns (i.e., B.1 and B.2) and the experiment by Torres et al., 2018. The circles colored in yellow and red mark the moments when the output sulfate concentrations reached values higher than 500 mg/L and 1000 mg/L, respectively. The dotted line in Torres et al., 2018 correspond to modeled data.

4. Conclusions, implications and future challenges

The present study has shown how other sources of CaCO₃ (i.e., mussel shells, clams shells and eggshells) might be as efficient (or even more) than limestone to remove Fe, Al and Cu from AMD polluted waters. These observations could facilitate the improvement of the DAS technology environmental footprint by reusing alternative by-product or residues (instead of mining raw materials) from local industries closer to the future full-scale treatment locations. However, to really consider these replacement alkaline reagents as more sustainable options than limestone, it is always necessary to perform a Life Cycle Assessment (LCA) including the whole context of the specific site where a passive treatment could be implemented.

It is also important to notice that, for the first time, malachite has been confirmed as a mineral actively involved in the AMD remediation processes. This observation is of a great importance for the optimum implementation of the DAS technology in AMDs with low to medium metal contents, because the mineralogical/geochemical reactions involved in the remediation process may be more diverse than previously thought. Also, it is important to notice that malachite stability highly depends on water pH (malachite equilibrium pH is around 7, depending on the water chemistry). Therefore, if a low-pH front migrates down the treatment system (as calcite is exhausted through

1
2
3
4 543 the months) malachite will be unstable and it will become a pollution source. Something similar
5 544 to what has been reported for hydrobasaluminite (equilibrium pH of 4.5). Consequently, it was
6 545 confirmed that the implementation of a DAS-type technology is not straightforward, not only
7 546 because the few operational parameters that have to be optimized and its working ranges defined
8 547 (i.e., residence time, flowrate that can be treated or the reagent useful lifetime) but also because of
9 548 new geochemical and mineralogical reaction that may be involved depending on the precise
10 549 elemental composition and elemental ratio of the AMD to be treated.
11
12
13
14 550

15 551 Taking into consideration present and previous results, the BaCO₃-DAS reagent lifetime clearly
16 552 depends on the sulfate load entering the system (i.e., higher sulfate loads = lower lifetime of the
17 553 reagent material; Fig. 5). Despite the observed generation of preferential flow paths within the
18 554 BaCO₃-DAS columns, most of the available witherite was completely or almost completely
19 555 consumed in the different sections of the columns (Table 4) achieving lifetimes of up to 6 months.
20 556 Therefore, although further investigations are necessary to avoid undesired preferential flow paths
21 557 within the reactive mixture, this optimization is not expected to significantly extend the lifetime
22 558 of the reactive mixture.
23
24
25 559

26 560 The guidance of previous experiences on upscaling DAS technology from laboratory-scale
27 561 experiments to full scale field passive treatment systems was used on the present discussion. The
28 562 reader is referred to previous works for more details about upscaling and field full-scale
29 563 implementation of DAS technology (Ayora et al., 2013; Martinez et al., 2019). Nonetheless, it is
30 564 worth to mention that the calculation of an even estimative cost for the full scale implementation
31 565 of this technology is highly dependent on many site-specific factors, like: 1) water chemistry, 2)
32 566 flowrate, 3) level of accessibility (or inaccessibility) of the construction site, 4) distance from the
33 567 chemical reagent and construction suppliers bases to the construction site, and 5) cost of civil
34 568 engineering works; just to mentioned a few. As a result, very different prices will arise for the
35 569 implementation of this technology on two full scale treatments at two very different realities. Just
36 570 to offer a made-up but realistic example, the reader can easily anticipate the very different costs
37 571 for the final implementation a of a full-scale treatment system in 1) Chile (in a high mountainous
38 572 inaccessible region with low acidity waters and low flowrate, for example) where just one or two
39 573 reactive tanks and decantation ponds may be needed to restore the water quality, or 2) Spain (in a
40 574 low mountainous accessible region with very high acidity waters and medium-low flowrate, for
41 575 example) where at least three much bigger reactive pools and decantation ponds may be necessary.
42 576 Building the first one (Capex) could be in the order of 500,000 US\$ while the second could be in
43 577 the order 1 to 2 million euros. The Opex of these made-up treatments would show even more
44 578 differences between them because the reagents consumption and treatment residues management
45 579 (main Opex costs) are highly variable depending on the metallic and sulfate loads of the waters,
46 580 and on the environmental legislation of each specific country.
47
48
49
50
51
52
53

54 581 To get a realistic estimate of the costs associated with the use of witherite as reagent material,
55 582 the following upscaling exercise is offered. To begin with, the accumulated removed sulfate load
56 583 per volume of reactive mixture at the end of the system optimal performance was calculated (Table
57 584 A.6, Appendix). This parameter ranged between 0.035 and 0.053 g of SO₄²⁻/cm³ of BaCO₃-DAS.
58 585 If it is assumed that the reactive mixture presents the same performance at field full-scale and
59
60
61
62
63
64
65

1
2
3
4
5
6
7
8
9
10
11
12
13
14
15
16
17
18
19
20
21
22
23
24
25
26
27
28
29
30
31
32
33
34
35
36
37
38
39
40
41
42
43
44
45
46
47
48
49
50
51
52
53
54
55
56
57
58
59
60
61
62
63
64
65

AMDs with the same compositions of the present study have to be remediated, a 1,000 m³ reactive pool (20m x 25m x 2,5m; length x width x depth) would be able to treat water inflows ranging from 3.3 to 11.8 L/s. This inflow rate is too low to remediate AMDs at active mine sites that typically exhibit flowrate of tens to hundreds of L/s. However, it perfectly fits the needs of abandoned and/or closed mine sites where the flow rates typically range between a few units to a few tens of L/s. Following this exercise and considering a cost of the commercial BaCO₃ reagent of 300 US\$/t (<https://www.alibaba.com/showroom/barium-carbonate-price.html>), the cost of the needed BaCO₃ for the reactive pool treating 3.3 L/s of AMD would be around 50,000 US\$. BaCO₃ current high price can be a serious obstacle for the economic feasibility of these type of passive treatment systems. However, several studies are setting the ground for the transformation of barite (BaSO₄) into witherite (BaCO₃) using a chemical engineering process based on the thermal reduction of BaSO₄ and CaCO₃ (combustion at 1,050 °C in the presence of coal) transforming BaSO₄ into BaS. The bubbling of CO₂ in the resulting BaS aqueous slurry finally produce BaCO₃ and S (Masukume et al., 2013; Mulopo, 2015). Since the final residue of the BaCO₃-DAS treatment is rich in both barite and calcite, the regeneration of this material could be a plausible option to improve the economic feasibility of the project under a circular economy perspective. The addition of a BaCO₃ regeneration process would affect both the OPEX and sustainability of the passive treatment, and a detail life cycle assessment of the specific final treatment configuration should be performed (to evaluate the feasibility of the new technological solution).

5. Acknowledgments

This study was funded by CORFO and Sacyr Chile through the project 16COTE-60128. It was also partially financed by the projects CONICYT/PIA Project AFB180004, FONDECYT Initiation Project 11150002 and FONDEQUIP (Project EQM130119). The authors thank Mario Jara for their analytical assistance. The authors thank Dr. Panos Seferlis (Associate Editor) and three anonymous reviewers for their suggestions and comments that significantly improved the quality of the original manuscript.

6. References

Akcil, A., &Koldas, S. (2006). Acid Mine Drainage (AMD): causes, treatment and case studies. *Journal of cleaner production*, 14(12-13), 1139-1145.

Ayora, C., Caraballo, M. A., Macias, F., Rötting, T. S., Carrera, J., & Nieto, J. M. (2013). Acid mine drainage in the Iberian Pyrite Belt: 2. Lessons learned from recent passive remediation experiences. *Environmental Science and Pollution Research*, 20(11), 7837-7853.

Barra, F., Reich, M., Selby, D., Rojas, P., Simon, A., Salazar, E., & Palma, G. (2017). Unraveling the origin of the Andean IOCG clan: A Re-Os isotope approach. *Ore Geology Reviews*, 81, 62-78.

1
2
3
4 623 Bavandpour, F., Zou, Y., He, Y., Saeed, T., Sun, Y., and Sun, G. (2018). Removal of dissolved
5 624 metals in wetland columns filled with shell grits and plant biomass, *Chemical Engineering*
6 625 *Journal*, 331, 234-241.
7
8
9 626 Camus, F., & Dilles, J. H. (2001). A special issue devoted to porphyry copper deposits of northern
10 627 Chile. *Economic Geology*, 96(2), 233-237.
11
12 628 Caraballo, M. A., Rötting, T. S., Nieto, J. M., & Ayora, C. (2009). Sequential extraction and DXRD
13 629 applicability to poorly crystalline Fe- and Al-phase characterization from an acid mine water
14 630 passive remediation system. *American Mineralogist*, 94(7), 1029-1038.
15
16 631
17 632 Caraballo, M. A., Macías, F., Nieto, J. M., Castillo, J., Quispe, D., & Ayora, C. (2011).
18 633 Hydrochemical performance and mineralogical evolution of a dispersed alkaline substrate (DAS)
19 634 remediating the highly polluted acid mine drainage in the full-scale passive treatment of Mina
20 635 Esperanza (SW Spain). *American Mineralogist*, 96(8-9), 1270-1277.
21
22
23 636 Delgado, J., Barba-Brioso, C., Ayala, D., Boski, T., Torres, S., Calderon, E., Lopez, F., 2019.
24 637 Remediation experiment of Ecuadorian acid mine drainage: geochemical models of dissolved
25 638 species and secondary minerals saturation. *Env. Sci. and Pollut. Research* 26, 34854–34872.
26 639 <https://doi.org/10.1007/s11356-019-06539-3>.
27
28 640
29 641 Dold, B. (2014). Evolution of acid mine drainage formation in sulphidic mine
30 642 tailings. *Minerals*, 4(3), 621-641.
31
32
33 643 FAO, 2018. Global Aquaculture Production 1950-2016 Database. Available at:
34 644 <http://www.fao.org/fishery/statistics/global-aquaculture-production/query/es>
35
36 645
37 646 Gazea, B., Adam, K., & Kontopoulos, A. (1996). A review of passive systems for the treatment of
38 647 acid mine drainage. *Minerals engineering*, 9(1), 23-42.
39
40 648
41 649 INAP, 2003. Treatment of Sulfate in Mine Effluents. International Network for Acid Prevention.
42 650 LORAX Environmental Inc. October, 2003. Retrieved from:
43 651 http://www.inap.com.au/public_downloads/Research_Projects/Treatment_of_Sulphate_in_Mine
44 652 [_Effluents_-_Lorax_Report.pdf](http://www.inap.com.au/public_downloads/Research_Projects/Treatment_of_Sulphate_in_Mine)
45
46
47 653 Jacobs, J. A., Lehr, J. H., & Testa, S. M. (2014). *Acid mine drainage, rock drainage, and acid*
48 654 *sulfate soils: causes, assessment, prediction, prevention, and remediation*. John Wiley & Sons.
49
50 655 Johnson, D. B., & Hallberg, K. B. (2005). Acid mine drainage remediation options: a
51 656 review. *Science of the total environment*, 338(1-2), 3-14.
52
53 657
54 658 Kefeni, K. K., Msagati, T. A., & Mamba, B. B. (2017). Acid mine drainage: prevention, treatment
55 659 options, and resource recovery: a review. *Journal of Cleaner Production*, 151, 475-493.
56
57 660 Macías, F., Caraballo, M. A., Rötting, T. S., Pérez-López, R., Nieto, J. M., & Ayora, C. (2012).
58 661 From highly polluted Zn-rich acid mine drainage to non-metallic waters: Implementation of a
59
60
61
62
63
64
65

1
2
3
4
5
6
7
8
9
10
11
12
13
14
15
16
17
18
19
20
21
22
23
24
25
26
27
28
29
30
31
32
33
34
35
36
37
38
39
40
41
42
43
44
45
46
47
48
49
50
51
52
53
54
55
56
57
58
59
60
61
62
63
64
65

662 multi-step alkaline passive treatment system to remediate metal pollution. *Science of the total*
663 *environment*, 433, 323-330.

664
665 Martínez, N. M., Basallote, M. D., Meyer, A., Cánovas, C. R., Macías, F., & Schneider, P. (2019).
666 Life cycle assessment of a passive remediation system for acid mine drainage: Towards more
667 sustainable mining activity. *Journal of Cleaner Production*, 211, 1100-1111.

668 Martínez-Garcia, C., Gonzalez-Fonteboa, B., Martinez-Abella, F. and Carro- Lopez, D. (2017).
669 Performance of mussel shell as aggregate in plain concrete. *Construction Building Materials*,
670 139,570-583.

671 Martínez-Garcia, C., Gonzalez-Fonteboa, B., Carro-Lopez, D., and Martinez-Abella, F. (2019). 8
672 - Recycled mollusc shells, Editor(s): Jorge de Brito, Francisco Agrela, In Woodhead Publishing
673 Series in Civil and Structural Engineering, New Trends in Eco-efficient and Recycled Concrete,
674 Woodhead Publishing, pages 191-205, ISBN 9780081024805, [https://doi.org/10.1016/B978-0-08-](https://doi.org/10.1016/B978-0-08-102480-5.00008-7)
675 [102480-5.00008-7](https://doi.org/10.1016/B978-0-08-102480-5.00008-7).

676 Masukume, M., Maree, J.P., Ruto, S., Joubert, H., 2013. Processing of barium sulphide to barium
677 carbonate and sulphur. *Chem. Eng. Proc. Technol.* 4, 157. [https://doi.org/10.4172/2157-](https://doi.org/10.4172/2157-7048.1000157)
678 [7048.1000157](https://doi.org/10.4172/2157-7048.1000157).

679 Mulopo, J., 2015. Continuous pilot scale assessment of the alkaline barium calcium desalination
680 process for acid mine drainage treatment. *J. Environ. Chem. Eng.* 3, 1298-1302.

681 Parkhurst, D. L., &Appelo, C. A. J. (2013). *Description of input and examples for PHREEQC*
682 *version 3: a computer program for speciation, batch-reaction, one-dimensional transport, and*
683 *inverse geochemical calculations* (No. 6-A43). US Geological Survey.

684 Rose, A.W., D. Bisko, A. Daniel, M.A. Bower, and S. Heckman. 2004. An “autopsy” of the failed
685 Tangaskootack #1 vertical flow pond, Clinton Co., Pennsylvania. p. 1580–1594. In R.I. Barnhisel
686 (ed.) Joint Conference of the 21st Annual Meetings of the American Society of Mining and
687 Reclamation and 25th West Virginia Surface Mine Drainage Task Force Symposium,
688 Morgantown, WV. ASMR, Lexington, KY.

689
690 Rötting, T. S., Thomas, R. C., Ayora, C., & Carrera, J. (2006a). Challenges of passive treatment
691 of metal mine drainage in the Iberian Pyrite Belt (Southern Spain): preliminary studies. In *Proc.*
692 *of the Seventh Int. Conf. on Acid Rock Drainage, St. Louis, MO* (pp. 1753-1767).

693 Rötting, T. S., Cama, J., Ayora, C., Cortina, J. L., & De Pablo, J. (2006b). Use of caustic magnesia
694 to remove cadmium, nickel, and cobalt from water in passive treatment systems: column
695 experiments. *Environmental science & technology*, 40(20), 6438-6443.

696
697 Rötting TS, Thomas RC, Ayora C, Carrera J (2008a) Passive treatment of acid mine drainage with
698 high metal concentrations using dispersed alkaline substrate. *J Environ Qual* 37:1741–1751

1
2
3
4
5
6
7
8
9
10
11
12
13
14
15
16
17
18
19
20
21
22
23
24
25
26
27
28
29
30
31
32
33
34
35
36
37
38
39
40
41
42
43
44
45
46
47
48
49
50
51
52
53
54
55
56
57
58
59
60
61
62
63
64
65

Rakotonimaro, T.V., Neculita, C.M., Bussière, B., Zagury, G.J., 2016. Effectiveness of various dispersed alkaline substrates for the pretreatment of ferriferous acid mine drainage. *Appl. Geochem.* 73, 13–23.

Rakotonimaro, T.V., Neculita, C.M., Bussière, Genty, T., B., Zagury, G.J., 2018. Performance assessment of laboratory and field-scale multi-step passive treatment of iron-rich acid mine drainage for design improvement. *Env. Sci. and Pollut. Research* 25, 17575–17589. <https://doi.org/10.1007/s11356-018-1820-x>

Sheoran, A. S., &Sheoran, V. (2006). Heavy metal removal mechanism of acid mine drainage in wetlands: a critical review. *Minerals engineering*, 19(2), 105-116.

Simón, M., Martín, F., García, I., Bouza, P., Dorronsoro, C., & Aguilar, J. (2005). Interaction of limestone grains and acidic solutions from the oxidation of pyrite tailings. *Environmental pollution*, 135(1), 65-72.

Skousen, J., &Ziemkiewicz, P. (2005). Performance of 116 passive treatment systems for acid mine drainage. *Proceedings, American Society of Mining and Reclamation, Breckenridge, CO*, 1100-1133.

Skousen, J., Zipper, C. E., Rose, A., Ziemkiewicz, P. F., Nairn, R., McDonald, L. M., &Kleinmann, R. L. (2017). Review of passive systems for acid mine drainage treatment. *Mine Water and the Environment*, 36(1), 133-153.

Torres, E., Lozano, A., Macías, F., Gomez-Arias, A., Castillo, J., & Ayora, C. (2018). Passive elimination of sulfate and metals from acid mine drainage using combined limestone and barium carbonate systems. *Journal of Cleaner Production*, 182, 114-123.

USEPA. U.S. Environmental Protection Agency, 2017. National Drinking Water Regulations. Retrieved from. <https://www.epa.gov/dwstandardsregulations>.

Valenzuela, M (2019). MsCminingthesis “*Monitoreo ambiental y análisis espacio temporal de la calidad hídrica de la cuenca del Mapocho*”. Graduated. Universidad de Chile, Santiago

WHO, World Health Organization, 2008. Guidelines for Drinking-water Quality. Fourth Edition. Retrieved from. http://www.who.int/water_sanitation_health/dwq/fulltext.pdf.

Younger PL, Banwart SA, Hedin RS (2002) Mine water: hydrology, pollution, remediation. Kluwer, Dordrecht, 442 pp.

Younger PL, Wolkersdorfer C (2004) Mining impacts on the fresh water environment: technical and managerial guidelines for catchment scale management. *Mine Water Environ* 23:s2–s80

Ziemkiewicz, P.F., Skousen, J.G., Simmons, J., 2003. Long-term performance of passive acid mine drainage treatment systems. *Mine Water and the Environment* 22, 118-129.